

Vibration analysis of a flexible crane hoist beam under harmonic unbalance excitation

Bernard Xavier Tchomeni kouejou ^{1*}, Filipeson Sozinando Desejo ¹, and Alfayo Anyika Alugongo¹

¹ Vaal University of Technology, Vanderbijlpark, Department of Industrial Engineering, Operations Management and Mechanical Engineering, South Africa,

Abstract. This study develops a three-degree-of-freedom nonlinear dynamic model for a flexible crane hoist system subjected to deterministic harmonic unbalance. Unlike conventional crane models that assume rigid beams or prescribed trolley motion, the current formulation explicitly incorporates beam flexibility and deterministic unbalance within a coupled nonlinear framework. The model integrates trolley displacement, payload swing, and the first bending mode response of the supporting beam to capture the key features of the coupled electromechanical–structural interaction. Lagrangian mechanics is used to derive the governing equations, and numerical simulations reveal low-amplitude, multi-frequency trolley motion, a dominant pendulum oscillation at low frequencies, and high-frequency beam bending effects associated with the unbalanced motor. Frequency analysis identifies distinct peaks related to the pendulum, beam, and excitation frequencies, illustrating the resonance mechanisms that appear when structural flexibility is considered. The results show that the beam’s flexibility significantly influences the dynamic response, modulates trolley motion, and amplifies high-frequency components during lifting. This study contributes to understanding the influence of deterministic excitation on the dynamics of overhead cranes and provides a structured framework for evaluating vibrations in flexible lifting systems.

1 Introduction

A crane is a machine that lifts, transports, and unloads heavy loads and is widely used across various industries, including construction, maritime, ports, warehousing, and agriculture, where heavy loads fluctuate frequently, and safe handling is essential. Crucial in these sectors, cranes effectively manage changing load conditions that influence response times and system stability. A shift in the system's position generates information about loads that affect the system's response time in engineering scenarios. When loads of this type impact the system, it reacts dynamically to the displacement caused by variations in the load's position and magnitude.

Cranes are generally equipped with a hoist or a wire rope drum, chains, and sheaves to move vertically or horizontally beyond human capability. This machine has proven instrumental in aiding humans with the handling of loads that surpass their individual capabilities. The ancient Greeks and Romans pioneered the development of cranes for the purpose of lifting heavy weights [1]. The ancient Greeks pioneered the replacement of booms with pulley and winch systems to lift large stones and build monumental structures. More advanced harbor cranes appeared in medieval Europe, some mounted on stone towers for greater stability [2]. During the industrial revolution, iron and steel replaced wood as the main building materials, increasing durability and load capacity [3]. Early cranes operated with human or animal power, and historical records

show that the ancient Greeks used such mechanisms to construct towering structures. Later, more sophisticated cranes employed human treadwheels, greatly boosting their lifting capabilities for larger objects. Harbor cranes, mainly used for loading, unloading ships, and construction, were strategically placed, with some built inside stone towers for added strength and stability. Initially, cranes were primarily made from timber. However, with the industrial revolution, materials like cast iron, iron, and steel became dominant in crane manufacturing [3]. The earliest cranes relied on manual or animal labor for power. In the 18th and 19th centuries, the invention of steam engines revolutionized crane operation, which remained a common power source until the late 20th century. Today, cranes are often powered by internal combustion engines, electric motors, or hydraulic systems to enhance lifting capacity [4]. Millions of cranes operate worldwide, valued for their ability to carry heavy materials. They are used in various settings such as construction sites, warehouses, and docks. Cranes come in many shapes and sizes, each designed for specific tasks. Besides jib cranes, which are used in workplaces, and tower cranes, essential in constructing large buildings, there are also mini cranes for working in tight or hard-to-reach areas [5]. Cranes can be modeled as underactuated Lagrangian systems, as suggested by [6]. For example, two-dimensional gantry cranes fit within this framework because they have fewer control actuators than degrees of freedom (DOF). In such systems, a single motor controls both the

* Corresponding author: bernardt@vut.ac.za

cart's position on the girder and the oscillation of the load. Cranes are classified as Lagrangian systems and are related to robotic manipulators, based on the application of Lagrangian mechanics to describe their motion. This allows for a thorough understanding of their behavior using mathematical models. To prevent load oscillations and ensure safe operation, advanced adaptive control techniques are essential [7-8]. A crane system, a highly complex engineering structure, consists of two main parts: the structural support and the hoisting mechanisms. These elements work together to facilitate movement during operation. The hoisting mechanism is especially important because it exhibits oscillatory behavior due to the inherent underactuation of the system. This underactuation means the crane has fewer control inputs than the DOF, making precise control more challenging. Cranes generally operate as underactuated Lagrangian systems in which a single actuator controls both the horizontal movement of the trolley and the pendulum behavior of the suspended load. This intrinsic coupling generates oscillations that affect the safety, positioning accuracy, and fatigue of structural components. According to [9], related experimental work on cracked Cardan shaft systems operating under viscous hydrodynamic forces further illustrates how structural defects and fluid-induced damping can reshape vibration patterns, reinforcing the broader relevance of understanding coupled, flexible, and fault-sensitive dynamics such as those examined in the present crane hoist model.

Faced with increasing demands for lifting speed and operational efficiency, it has become essential to understand the vibration characteristics of flexible girder crane systems. Structural flexibility modifies load–motion interactions, introduces additional vibration modes, and influences resonance mechanisms. Existing dynamic models of overhead cranes often neglect structural flexibility or consider trolley movement as predefined, which limits their ability to understand resonance and frequency coupling phenomena. Furthermore, deterministic unbalanced excitation due to rotating machines is rarely explicitly considered. The present study addresses these gaps by developing a coupled trolley-pendulum-beam model that takes into account beam bending and unbalanced harmonic excitation. This research also examines a crane lifting system in which a mobile motor exhibiting deterministic unbalance excites both the beam and the suspended load.

This article consists of the following sections: The second section describes the crane lifting system. The third section presents the analytical solutions, natural frequency, and modal form of the proposed model. In the fourth section, mathematical simulation and the results of the third are presented. Finally, the fifth section, the conclusion and future work, is written.

2 Dynamic equation of the excited beam

2.1 Model description and foundational assumptions

Figure 1 illustrates the schematic configuration of an electric hoist. It features a set of interconnected components, including the power source (electric motor), the lifting mechanism (hoist, drum, wire rope, hook), the transport trolley, the structure (bridge, runway, mast), the control system, and the load itself. All of these components work together to lift and move heavy materials.

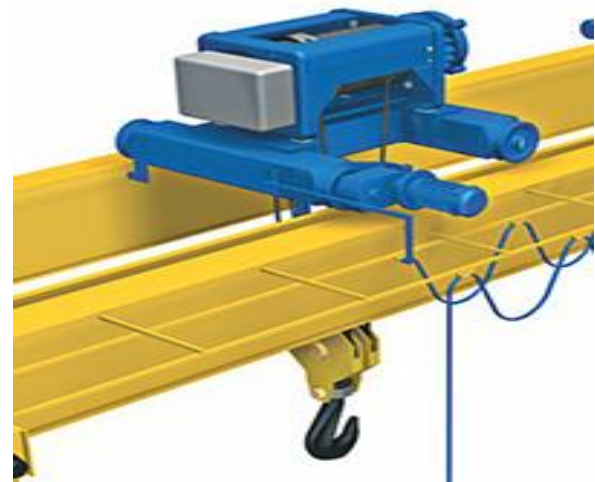


Fig.1 Physical system of electric crane hoist

The foundational assumptions underpinning the formulation of the equation of motion for the unbalanced crane hoist system are delineated as follows:

- The beam is uniformly structured and exhibits simple support at both extremities. This assumption is justified by the low-frequency excitation range considered.
- Both the beam and motor are characterized by elastic behavior, with consideration given solely to transverse deflection.
- Shear stresses and transverse normal strains are neglected in the system.
- The assumption is made that the plane sections of the beam remain planar throughout deformation, and any resulting beam slopes are assumed to be small.
- The influence of the rope, connected to the centerline of the motor, is omitted from consideration to focus on the dominant structure-pendulum coupling mechanisms at the beam level.

Based on the assumptions discussed above, the unbalanced crane hoist system results in the following equations:

$$EI \frac{\partial^4 w(x,t)}{\partial x^4} + \rho A \frac{\partial^2 w(x,t)}{\partial t^2} = f(x,t) \quad (1)$$

Where E is Young's modulus, I is the second moment of the cross-section of the beam, ρ is the density of the material, A is the cross-sectional area, and $f(x,t)$ represents the external load per unit length. The expression denoted as Equation (1) encapsulates the equation of motion governing the beam's response to

external forces or displacements. The solution to this equation is posited as a linear combination of the normal modes based on a fundamental hypothesis. This linear combination enables the representation of the beam's displacement as the cumulative effect of contributions from each mode. This assumption aligns with the principle of superposition, which asserts that the response of a linear system to multiple inputs can be derived by aggregating the responses corresponding to each input.

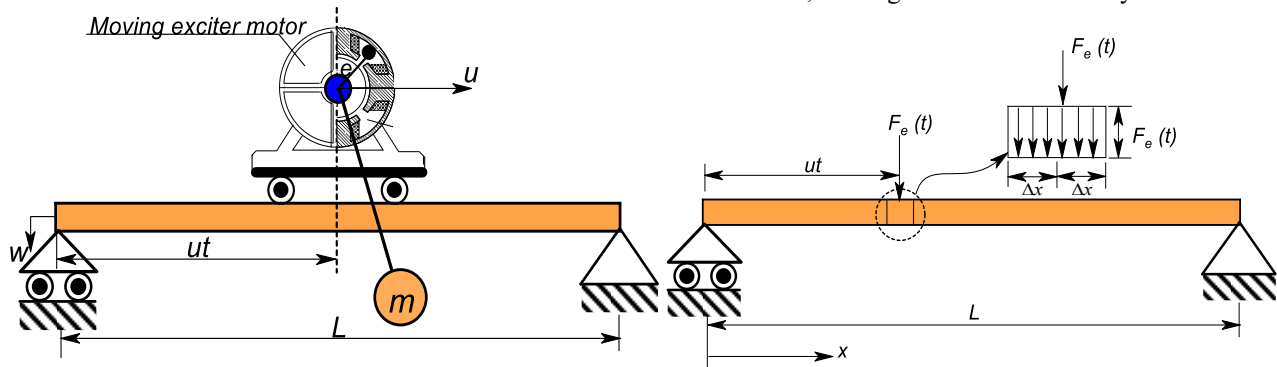


Fig. 2. (a) Kinematic representation of a trolley-motor assembly moving on a flexible beam, where the motor exhibits a deterministic harmonic unbalance; (b) Equivalent dynamic model of the simply supported beam under an unbalance.

When a simple support supports a beam, it is characterized by a set of boundary conditions that include:

$$w(0, t) = 0 \quad (3)$$

$$\frac{\partial^2 w}{\partial x^2}(0, t) = 0 \quad (4)$$

$$w(L, t) = 0 \quad (5)$$

$$\frac{\partial^2 w}{\partial x^2}(L, t) = 0 \quad (6)$$

Where L is the beam span. These assumptions are consistent with typical overhead crane runway or lifting beam installations and allow for an analytical modal representation. In the current configuration, the beam is assumed to be simply supported at both ends, which leads to the following boundary conditions:

$$w(x, 0) = 0 \quad (7)$$

$$\frac{\partial w}{\partial x}(x, 0) = 0 \quad (8)$$

2.2 Modal reduction of the beam dynamics

To obtain a usable representation suitable for coupling with the trolley-pendulum system, the beam displacement is expressed as a modal development.

$$w(x, t) = \sum_{n=1}^{\infty} \phi_n(x) q_n(t) \quad (9)$$

where $\phi_n(x)$ are the admissible operating modes satisfying the boundary conditions, and $q_n(t)$ are the corresponding generalized modal coordinates.

Mathematically, if we denote the displacement of the beam at a given point and time as $w(x, t)$, where x represents the position along the beam and t represents time, we can express it as:

$$w(x, t) = \sum_{i=1}^{\infty} W_i(x) \eta_i(t) \quad (2)$$

As illustrated in Figure 2, the beam is excited by a trolley carrying a motor with deterministic harmonic unbalance, moving at a constant velocity u .

For a simply supported beam, the natural modes and frequencies are given by:

$$\omega_n = \frac{n^2 \pi^2}{L^2} \sqrt{\frac{EI}{\rho A}} \quad (10)$$

and

$$\phi_n(x) = \sin\left(\frac{n\pi x}{L}\right) \quad (11)$$

In this study, only the first mode of bending is considered. The first bending mode is conserved because its natural frequency is closest to the excitation and swaying frequencies, while the higher modes are well separated and weakly excited under the operating conditions considered. In this single-mode approximation, the beam displacement is written as follows:

$$w(x, t) = \phi_1(x) q(t) \quad (12)$$

where $q(t)$ represents the generalized coordinate associated with the first mode of bending.

2.3 Reduced-order beam equation

By substituting the single-mode approximation in the equation governing the motion and applying the standard Galerkin projection, we obtain a reduced-order equation of motion of the following form:

$$M_b \ddot{q}(t) + C_b \dot{q}(t) + K_b q(t) = Q(t) \quad (13)$$

where M_b , C_b , and K_b respectively denote the generalized mass, damping, and stiffness associated with the first mode of the beam, and $Q(t)$ the corresponding generalized force.

In the current formulation, the generalized force $Q(t)$ results from the interaction between the moving cart and the flexible beam. This interaction force is determined by the relative motion between the trolley and the beam at the location of the trolley and is explicitly introduced into the coupled system equations presented in Section 4.

3 Natural frequency and mode shape

Each vibration mode represents an independent deformation pattern associated with a distinct natural frequency of the beam. The system exhibits harmonic vibrations that occur at the second natural frequency. Linear structures can be analyzed by breaking down their dynamic deflection shapes into basic vibration patterns. In this section, the modal analysis method was used to identify the natural frequencies and modal shapes of the structure, helping to understand its behavior. Higher modes are presented here only for completeness and validation, but are not included in the coupled dynamic simulations.

The solution of Equation (1) can be written in the following form:

$$W(x) = \begin{bmatrix} \Omega_1 & \Omega_2 & \Omega_3 & \Omega_4 \end{bmatrix} \begin{Bmatrix} C_1 \\ C_2 \\ C_3 \\ C_4 \end{Bmatrix} \quad (14)$$

where

$$\begin{bmatrix} \Omega_1 \\ \Omega_2 \\ \Omega_3 \\ \Omega_4 \end{bmatrix} = \begin{bmatrix} \cos(\beta x) + \cosh(\beta x) \\ \cos(\beta x) - \cosh(\beta x) \\ \sin(\beta x) + \sinh(\beta x) \\ \sin(\beta x) - \sinh(\beta x) \end{bmatrix} \quad (15)$$

As per Equation (14), it is apparent that the constants C_1 , C_2 , C_3 , and C_4 exhibit distinct values in each particular instance. Upon imposing the boundary conditions delineated in Equations (3) and (4), it is established that $C_1 = C_2 = 0$.

$$\begin{bmatrix} \Omega_3 & \Omega_4 \end{bmatrix} \begin{Bmatrix} C_3 \\ C_4 \end{Bmatrix} = 0 \quad (16)$$

$$\begin{bmatrix} -\Omega_3 & \Omega_4 \end{bmatrix} \begin{Bmatrix} C_3 \\ C_4 \end{Bmatrix} = 0 \quad (17)$$

In the context of Equations (16) and (17) and their respective coefficient matrix, it's recognized that C_3 and C_4 constitute a system of two equations with unknowns C_3 and C_4 . This system plays a pivotal role in comprehending and determining the coefficients in the provided equations.

To identify nontrivial values for C_3 and C_4 , a critical condition arises: the determinant of the coefficient matrix must be zero. This indicates that the system of

equations is linearly dependent, suggesting the existence of multiple or infinite solutions for the unknowns C_3 and C_4 . This condition holds significance in understanding the nature of solutions within this specific mathematical context.

$$\sin(\beta L) \sinh(\beta L) = 0 \quad (18)$$

In the context of the given Equation (18), it is evident upon observation that the function $\sinh(\beta L)$ does not attain a value of zero unless β is equal to zero. However, the value of $\beta = 0$ is not considered significant in this case. This is because when β equals zero, it implies that, according to Equation (18), the value of ω is also zero. The scenario corresponds to the beam being at rest. Therefore, the focus of analysis lies in cases where β does not equal zero, as these scenarios represent the beam's dynamic behavior. Thus, the frequency equation is as follows:

$$\sin(\beta L) = 0 \quad (19)$$

The roots of Equation (19), $\beta_n L$, are given by :

$$\beta_n L = n\pi \quad n = 1, 2, \dots \quad (20)$$

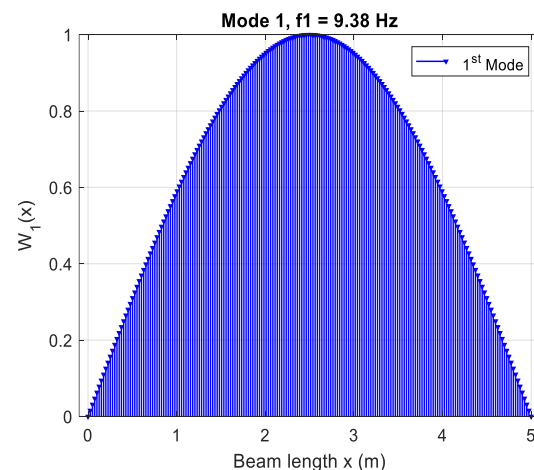
Consequently, the natural frequencies of vibration are then determined as follows:

$$\omega_n = n^2 \pi^2 \sqrt{\frac{EI}{\rho AL^4}} \quad n = 1, 2, \dots \quad (21)$$

Substituting (19) into (16), we find that $C_3 = C_4$. Hence, (14) gives the mode shape as:

$$W_n(x) = C_n \sin\left(\frac{n\pi x}{L}\right) \quad n = 1, 2, \dots \quad (22)$$

The first four vibration modes of the beam describe its deformation at different frequencies. By integrating them into the model, the differential equations of the crane lifting system change to a multi-degree-of-freedom system. The first four beam modes, shown in Figure 4, describe how the beam deforms at different frequencies.



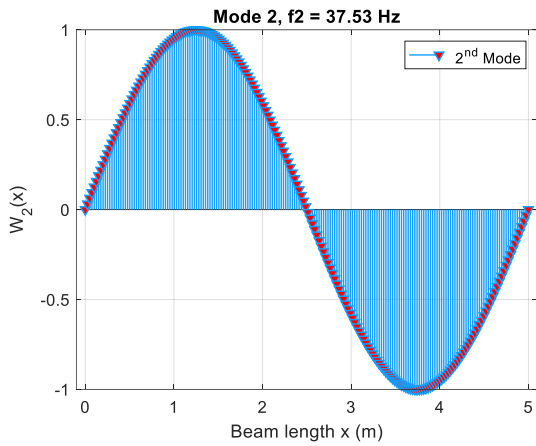


Fig. 3. Modal response of the beam's first and second mode.

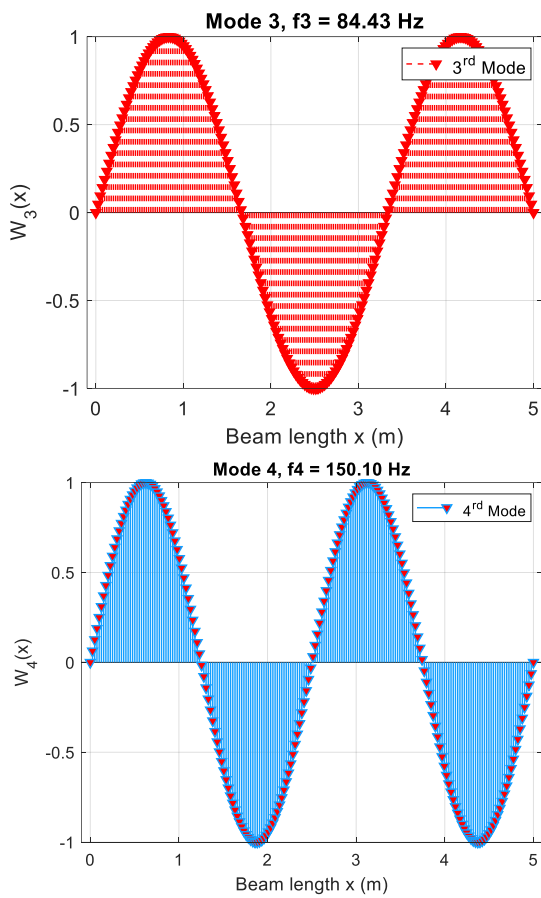
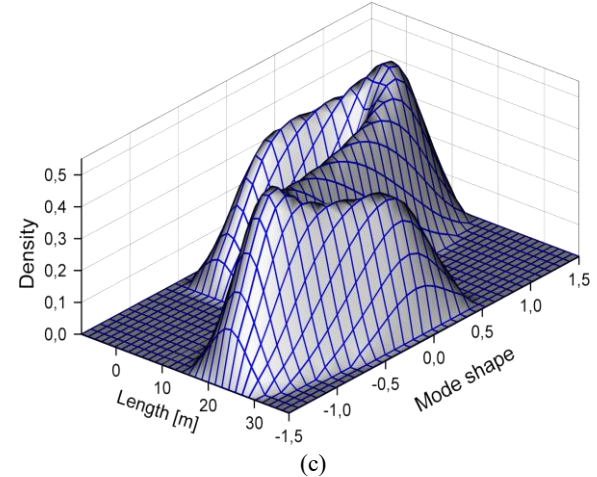
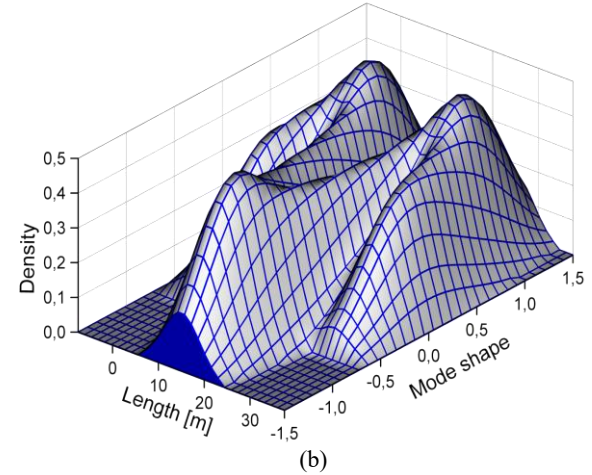
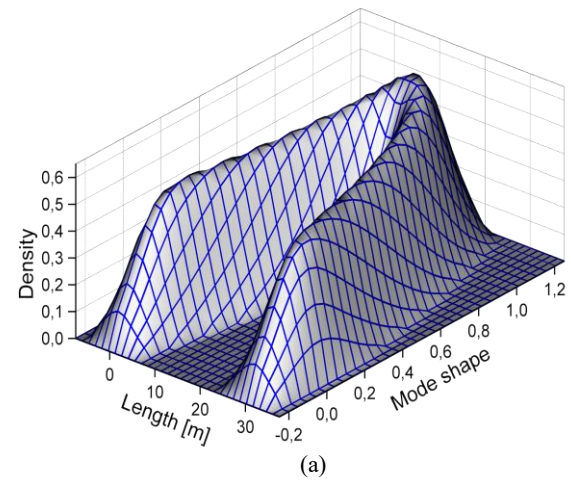


Fig. 4. Modal response of the beam's third and fourth mode.

The inclusion of the mode shape into the crane hoist, including the first beam mode (multi-modal beam coordinate), expands the hoist ODEs from a two-degree-of-freedom system to a multi-degree-of-freedom system, where the basic motion $y(t)$ of the trolley is no longer predefined but is represented as a modal expansion. The lower modes dominate, but higher modes can become significant if the exciter frequency or external loads match their natural frequencies.

The analysis of the four vibration modes of the beam, illustrated in Figure 3 and Figure 4, shows that, for a simply supported beam, the first four vibration modes,

classified by increasing frequency, are as follows: mode 1, with the lowest frequency, presents a half-sine wave with maximum deflection in the middle of the beam; it determines the overall response to bending. Mode 2 forms a full sine wave with a node in the middle of the beam, making it more sensitive to off-center loads and contributing to asymmetric vibrations (Fig. 3). Mode 3 consists of three half-waves, producing higher frequencies and multiple nodes, which is important for characterizing localized dynamic effects and responses to high-frequency excitations. Finally, mode 4 exhibits four half-waves at an even higher frequency, which allows characterizing the short-wavelength bending behavior, typically observed under high-frequency loads or shocks (Figure 4).



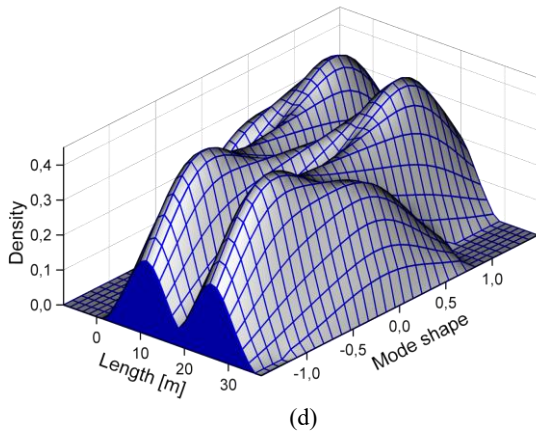


Fig. 5. Modal response of the beam's first four modes of vibration; (a) 1st mode; (b) 2nd mode; (c) 3rd mode; (d) 4th mode

Discussion 1

Figure 5 shows the first four modes of vibration for a supported crane beam representing different patterns of deformation when subjected to dynamic deterministic unbalance excitation. These modes are associated with different natural frequencies of the beam. Figure 5(a) represents the first mode with the lowest frequency and the primary mode of vibration. In this mode, the beam deforms into a single symmetric curve, forming a sinusoidal shape seen from the top view with a single peak. The beam bends in the shape of a half-sine wave, with the maximum deflection occurring at the centre and decreasing towards the supports. In Figure 5(b), the second mode, with the first higher frequency mode, has a nodal point at the centre of the beam. In this mode, the beam forms two symmetric curves, resembling two half-sine waves. The maximum deflections occur at points equidistant from the centre and decrease towards the supports. The beam undergoes a twisting motion as well as bending. Figure 5(c) shows the third mode, with the second-highest frequency mode, and has two nodal points, dividing the beam into three segments. In this mode, the beam forms three symmetric curves, similar to three half-sine waves. The maximum deflections occur at the nodal points, and the beam undergoes more complex bending and twisting deformations compared to the previous modes. Figure 5(d) shows that the fourth mode is the third-highest frequency mode and has three nodal points, dividing the beam into four segments. In this mode, the beam forms four symmetric curves, resembling four half-sine waves. The maximum deflections occur at the nodal points, and the beam undergoes more intricate bending and twisting deformations.

4 Governing equation of the unbalanced crane hoist system

4.1 Equation of the unbalanced crane hoist system

The crane hoist consists of a trolley of mass \mathbf{M} , a suspended load of mass \mathbf{m} , and an unbalanced rotating mass \mathbf{m}_e generating a deterministic excitation:

$$F_e(t) = m_e e \Omega^2 \cos(\Omega t). \quad (23)$$

The generalized coordinates are (i) trolley displacement $x(t)$, (ii) payload swing angle $\theta(t)$, and (iii) beam modal coordinate $w(t)$.

Hoist vibration systems use methods of storing potential energy (springs), kinetic energy (mass or inertia), and gradual energy loss (damper). Although a single physical structure can store and release both kinetic and potential energy, this section only deals with lumped parameter systems consisting of perfect springs, masses, and dampers, which have only one function. From Fig.2 (a), the moving foundation (beam) has a prescribed displacement $y(t)$ ($y = ut$ or base vibration). The vector position of mass m and the resulting squared velocity is given by:

$$\vec{s} = \begin{bmatrix} ut + L_r \sin \theta \\ x + L_r \cos \theta \end{bmatrix} \quad (24)$$

The general form of the kinetic energy of the system is given by:

$$T = \frac{1}{2} (M + m_e + m) \dot{x}^2 + mL_r \dot{x} \dot{\theta} \cos \theta + \frac{1}{2} mL_r^2 \dot{\theta}^2 \quad (25)$$

The system potential energy associated with gravity loading is given by:

$$U = \frac{1}{2} k (x - y_b(t))^2 + mgL_r (1 - \cos \theta) \quad (26)$$

Where $y_b(t)$ is the known input displacement of the beam/track at the trolley location.

The Rayleigh dissipated function represents the energy dissipated from the system associated with the damper can be expressed as:

$$R = \frac{1}{2} c (\dot{x} - \dot{y}_b(t))^2 \quad (27)$$

In the x -direction, the unbalanced force $F_e(t)$ acts on the trolley, plus base forcing transmitted by spring/damper is included in LHS via a defined coupling force once:

$F_{sd}(t) = c(\dot{x} - \dot{y}_b) + k(x - y_b)$. Using the Lagrange principle and appropriate calculation, the final equation of motion governing the vibration of the unbalanced hoist system shown in Figure 2(a) can be expressed in the matrix form as:

$$\begin{bmatrix} M + m + m_e & mL_r \cos \theta \\ mL_r \cos \theta & mL_r^2 \end{bmatrix} \begin{Bmatrix} \ddot{x} \\ \ddot{\theta} \end{Bmatrix} + \begin{bmatrix} c & 0 \\ 0 & 0 \end{bmatrix} \begin{Bmatrix} \dot{x} \\ \dot{\theta} \end{Bmatrix} + \begin{bmatrix} k & 0 \\ 0 & mgL_r \end{bmatrix} \begin{Bmatrix} x \\ \theta \end{Bmatrix} = \begin{Bmatrix} F_{sd}(t) + mL_r \dot{\theta}^2 \sin \theta + F_e(t) \\ mgL_r \sin \theta \end{Bmatrix} \quad (28)$$

where $y_b(t) = c(\dot{x} - \dot{y}_b) + k(x - y_b)$ is the force acting on the cart (positive when pushing the cart). The nonlinear terms arise from the geometric coupling between the translation of the cart and the rotation of the pendulum and include centrifugal and gravitational

restoring effects. The trolley is excited by deterministic unbalance $F_e(t)$ and coupled to the beam via $y_b(t)$. The $mL_r\dot{\theta}^2 \sin \theta$ term is an inertial or centrifugal term that appears in the trolley equation (first line) and results from the kinematics of the pendulum. The term $mgL_r \sin \theta$ is the nonlinear gravitational restoring torque in the pendulum equation.

4.2 The extended equation of the unbalanced crane hoist system with a single mode shape

According to Newton's third law, the beam receives the reaction force equal and opposite to the trolley spring-damper force: $F_{beam}(t) = -F_{sd}(t)$ at the location of the cart; the generalized modal force is obtained by multiplying the local force by the modal form ϕ , hence $-\phi F_{beam}(t)$. (ϕ is the beam mode shape evaluated at the trolley location). Rearrangement of the explicit beam coupling term in Equation (28):

$$M_b \ddot{w} + C_b \dot{w} + K_b w = -\phi(x) F_{sd}(t) \quad (29)$$

In the matrix form:

$$\begin{bmatrix} M + m + m_e & mL_r \cos \theta & 0 \\ mL_r \cos \theta & mL_r^2 & 0 \\ 0 & 0 & M_b \end{bmatrix} \begin{Bmatrix} \ddot{x} \\ \ddot{\theta} \\ \ddot{w} \end{Bmatrix} + \begin{bmatrix} c & 0 & -\phi c \\ 0 & 0 & 0 \\ -\phi c & 0 & C_b + \phi^2 c \end{bmatrix} \begin{Bmatrix} \dot{x} \\ \dot{\theta} \\ \dot{w} \end{Bmatrix} + \begin{bmatrix} k & 0 & -\phi k \\ 0 & 0 & 0 \\ -\phi k & 0 & K_b + \phi^2 k \end{bmatrix} \begin{Bmatrix} x \\ \theta \\ w \end{Bmatrix} = \begin{bmatrix} F_e(t) + \phi c \dot{w} + \phi k w \\ 0 \\ -\phi^2 (c \dot{w} + k w) \end{bmatrix} + \begin{bmatrix} mL_r \dot{\theta}^2 \sin \theta \\ mgL_r \sin \theta \\ 0 \end{bmatrix} \quad (30)$$

Equation (30) clearly shows that the interaction with the trolley modifies the effective modal damping and stiffness (adds $\phi^2 k$ and $\phi^2 c$) and couples the cart motion into the modal equation via $-\phi k x$ and $-\phi c \dot{x}$

4.3 Numerical integration and discussion

4.3.1 Crane hoist response at the first mode shape

The obtained equations were integrated using MATLAB. The coupled nonlinear equations were integrated using a fourth-order Runge–Kutta scheme with a fixed time step, ensuring numerical stability and

convergence. The initial conditions correspond to small perturbations around the equilibrium position. The system parameters are listed in Table 1. Simulations were performed for several excitation frequencies Ω .

Table 1. Initial values of system parameters

Parameter	Value
Young's modulus (E)	210 x 10 ⁹ N/m ²
Length of the beam (L)	5 m
First moment of area (I)	0.0093 m ⁴
Density (ρ)	7850 kg/m ³
Beam cross-sectional area (A)	0.128 m ²
Linear velocity (u)	2.778 m/s
Stiffness coefficient (k)	10 ⁸ N/m
Damping coefficient (c)	10 ⁵ Ns/m
Trolley mass (M)	20000 kg
Mass of payload (m)	20000 kg
Unbalance ($m_e e$)	0.1 kg·m

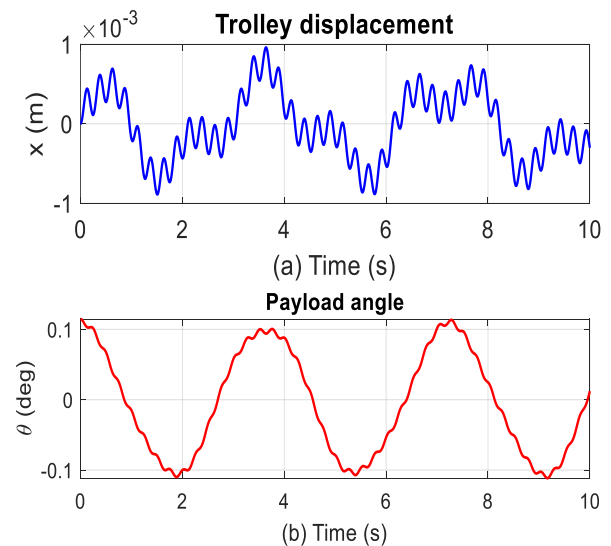


Fig. 6. Crane Hoist response under 1st mode beam vibration

The graphs shown in Figure 6(a) confirm that the trolley is rigid and exhibits low-amplitude vibrations. At the same time, the oscillatory motion of the load dominates the dynamic response at low frequencies. The coupling results in a mixing of frequencies in the trolley movement. In contrast, the pendulum movement is smoother and more pronounced (Figure 6(b)), which underlines the importance of controlling swing during lifting operations.

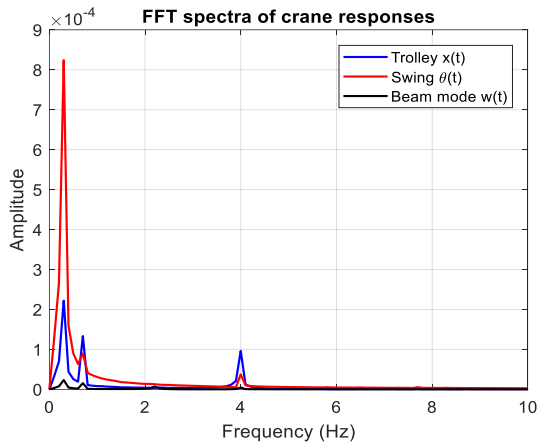


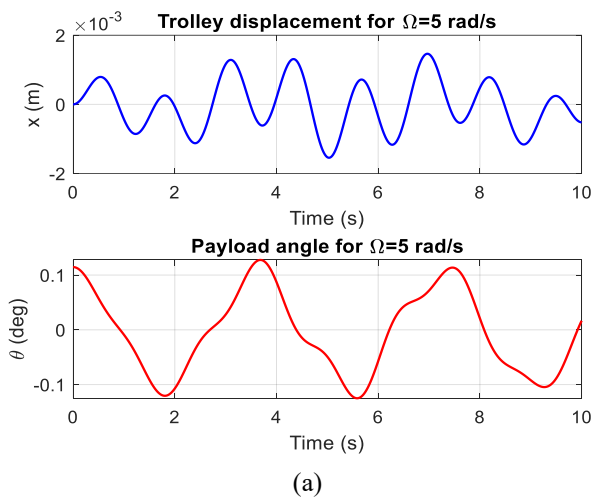
Fig. 7. Crane hoist natural frequency

The movement of the trolley $x(t)$ is influenced both by low-frequency coupling with the pendulum (amplitude modulation) and by high-frequency vibrations due to unbalance or external stress (ripples). The FFT shows

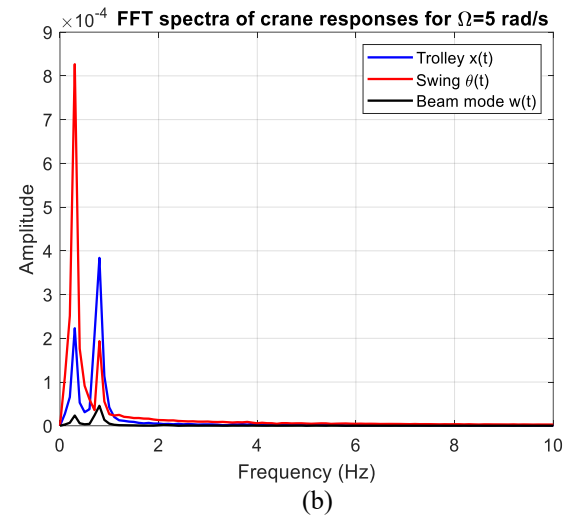
multiple peaks (low and high frequencies). In contrast, the signal $\theta(t)$ is mainly determined by the low-frequency dynamics of the pendulum; its FFT is concentrated around the pendulum frequency, with lower high-frequency content. The rotation of the exciter at an angular velocity of $\Omega = 25$ rad/s corresponds to an excited frequency f_{exc} of approximately 3.98 Hz (i.e., $25/(2\pi)$). The FFT plot shows a peak near 4 Hz, particularly visible in the spectra of the trolley position $x(t)$ (blue) and the beam deformation $w(t)$ (black), as shown in Figure 7.

4.3.2 Crane hoist response with varying excited force

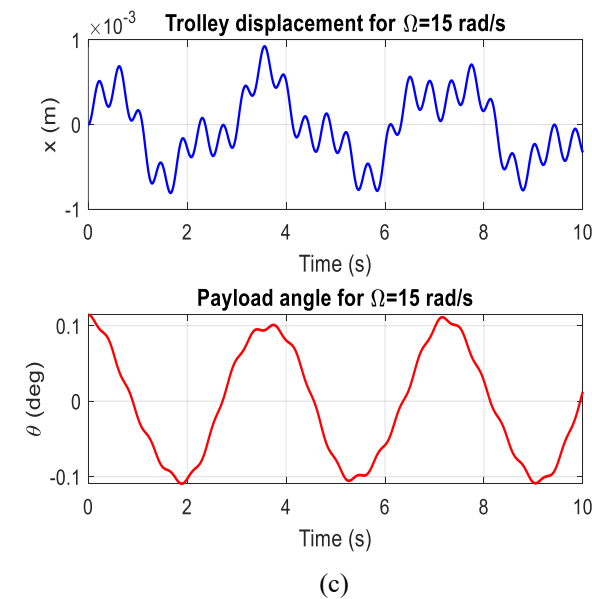
The analysis is performed with four different values of the angular velocity speed which correspond to the excited force. The responses of deflection and FFT are presented in Figure 8.



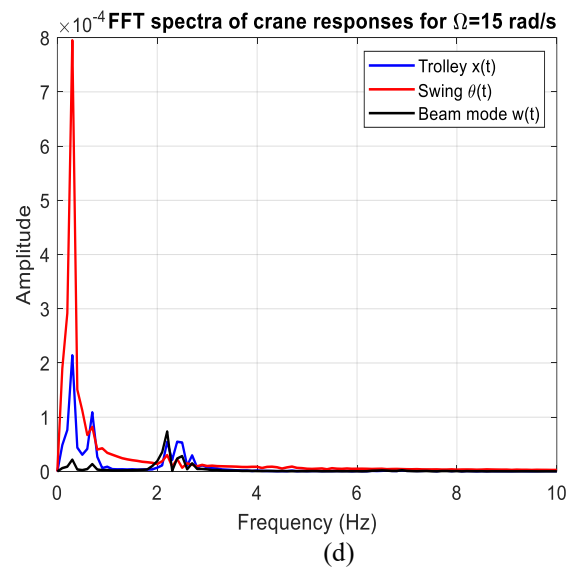
(a)



(b)



(c)



(d)

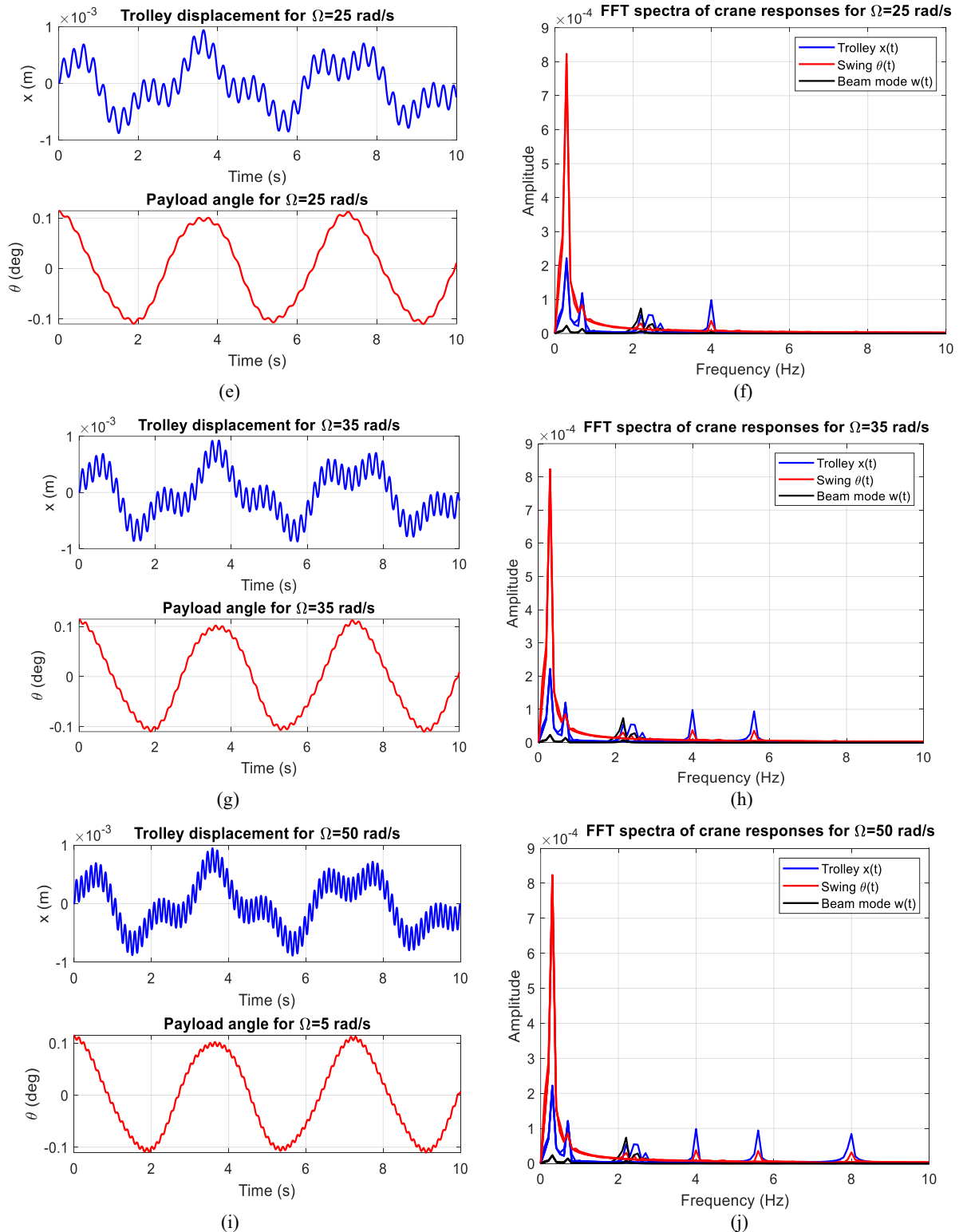


Fig. 8. Transverse deflection and FFT of the beam, (a) $\Omega = 5$ rad/s; (c) $\Omega = 15$ rad/s; (e) $\Omega = 25$ rad/s; (g) $\Omega = 35$ rad/s; (i) $\Omega = 50$ rad/s

Discussion 2

The main observation of this study is that when the first (dominant) vibration mode of the beam is excited, the displacement field of the system is characterized by a large modal component $w(t)$ and a local displacement of the base $\phi w(t)$. The payload reacts via the pendulum

coupling: the added inertia and the coupling term $mL_r \cos\theta$ generate a smaller but measurable displacement $x(t)$, as well as pendulum motion $\theta(t)$ induced by the double derivative of $w(t)$ via the coupling terms. Upon observation, the first mode displacement produces the largest spatially smooth deflection (largest amplitude at mid-range), dominates the low-frequency

structural response, and defines the baseline upon which the high-frequency unbalance forcing and pendulum oscillations are superimposed. Since the vibration mode of the beam is low frequency and often weakly damped, moderate harmonic excitation at nearby frequencies can generate a large displacement $w(t)$, leading to a positioning error of the trolley and a slow modulation of the pendulum motion (Figure 8(a), 8(c), 8(e), 8(g), and 8(i)). In Figure 8(b), 8(d), 8(f), 8(h), and 8(j), FFT analysis highlights the frequencies that carry the most energy and, therefore, the most influential physical parameters for controlling the crane's lifting system. A critical parameter is the excitation/eccentricity frequency Ω ; if it coincides with a natural frequency (pendulum f_p , beam f_{b1} , or coupled trolley-pendulum mode), a resonance appears as a large peak in the FFT

spectrum. It must be avoided or displaced by tuning. A distinct peak is observed at the beam bending frequency (first mode). As the trolley speed increases, the trolley vibrations transmit energy to the beam, so its spectrum may also contain harmonics of the unbalance frequency. Still, the largest contribution is near the beam's natural mode. From a practical point of view, the results indicate that beam flexibility can amplify high-frequency vibrations and must be taken into account in crane design and vibration control strategies. Therefore, the physical interpretation of any observed resonance or beating phenomenon must consider both the modal participation factors (e.g., ϕ , mL_r) and the nonlinear coupling terms that modulate the participation as the oscillations increase.

5 Conclusion

This study demonstrates that deterministic unbalance significantly influences the vibration response of a flexible overhead crane lifting system. Integrating beam flexibility reveals additional high-frequency behaviors and modifies the coupling between trolley movement and payload oscillation. Frequency analysis highlights key resonance interactions, providing insight into dynamic performance under harmonic excitation.

The main findings of the study can be summarized as follows:

1. The first modal shape of the beam, introduced by modal reduction, strongly influences the response of the trolley and couples the structural bending to the dynamics of the pendulum.
2. Time-domain results show that the trolley displacement is small but multi-frequency, with the pendulum motion dominating at low frequencies, while the modal beam displacement captures the high-frequency vibrations.
3. FFT analysis highlights dominant spectral peaks at the pendulum, beam, and exciter frequencies, allowing a clear understanding of the resonance mechanisms.

The present study is limited to planar motion and a single beam mode; future work will extend the model to include multiple modes, rope dynamics, and experimental validation

Reference

1. Seyhan IA. The early history of the pulleys and crane systems. *Foundations of Science*. 2024 Mar;29(1):87-103.
2. Pierattini A. Interpreting rope channels: lifting, setting and the birth of Greek monumental

architecture. *Annual of the British School at Athens*. 2019 Nov;114:167-206.

3. Evans C, Rydén G. The industrial revolution in iron: an introduction. In *The Industrial Revolution in Iron 2017 Jul 5* (pp. 1-14). Routledge.
4. KosucKi A, Stawiński Ł, Malenta P, Zaczyński J, Skowrońska J. Energy consumption and energy efficiency improvement of overhead crane's mechanisms. *Eksploracja i Niezawodność*. 2020;22(2):323-30.
5. Shapira A, Lucko G, Schexnayder CJ. Cranes for building construction projects. *Journal of Construction Engineering and Management*. 2007 Sep;133(9):690-700.
6. Molina-Santana E, Ferrer-Cepero MR, Gonzalez-Montañez F, Liceaga-Castro JU, Jimenez-Mondragon VM, Olivares-Galvan JC. Generalized framework for designing a linear control scheme for regulating a sub-actuated overhead crane. *International Journal of Dynamics and Control*. 2025 May;13(5):1-8.
7. Zhang, J., Wang, L., & Huang, T. Adaptive control of uncertain underactuated gantry cranes, *Journal of Engineering Control*, 33(7), pp. 995–1007(2019).
8. Liu, Y., Chen, Z., & Li, X, Dynamic modeling and oscillation suppression in underactuated crane systems, *Control Systems Reviews*, 55(4), pp. 221–239 (2023).
9. Tchomeni Kouejou BX, Alugongo AA. Experimental analysis of a cracked cardan shaft system under the influence of viscous hydrodynamic forces. *Fluids*. 2023 Jul 18;8(7):211.